



Contents lists available at ScienceDirect

Journal of Alloys and Compounds

journal homepage: www.elsevier.com/locate/jallcomDensity functional study of the $L1_0$ - α IrV transition in IrV and RhVMichael J. Mehl^{a,*}, Gus L.W. Hart^b, Stefano Curtarolo^c^a Center for Computational Materials Science, Naval Research Laboratory, Code 6390, Washington, DC 20375-5000, USA^b Department of Physics and Astronomy, Brigham Young University, Provo, UT 84602, USA^c Department of Mechanical Engineering and Materials Science and Department of Physics, Duke University, Durham, NC 27708, USA

ARTICLE INFO

Article history:

Received 1 June 2010

Received in revised form 11 August 2010

Accepted 23 August 2010

Available online 16 October 2010

Keywords:

Structural phase transitions

Jahn–Teller

Electronic structure

Density functional theory

Ordered intermetallic alloys

ABSTRACT

Both IrV and RhV crystallize in the α IrV structure, with a transition to the higher symmetry $L1_0$ structure at high temperature, or with the addition of excess Ir or Rh. Here we present evidence that this transition is driven by the lowering of the electronic density of states at the Fermi level of the α IrV structure. The transition has long been thought to be second order, with a simple doubling of the $L1_0$ unit cell due to an unstable phonon at the R point (0 1/2 1/2). We use first-principles calculations to show that all phonons at the R point are, in fact, stable, but do find a region of reciprocal space where the $L1_0$ structure has unstable (imaginary frequency) phonons. We use the frozen phonon method to examine two of these modes, relaxing the structures associated with the unstable phonon modes to obtain new structures which are lower in energy than $L1_0$ but still above α IrV. We examine the phonon spectra of these structures as well, looking for instabilities, and find further instabilities, and more relaxed structures, all of which have energies above the α IrV phase. In addition, we find that all of the relaxed structures, stable and unstable, have a density comparable to the $L1_0$ phase (and less than the α IrV phase), so that any transition from one of these structures to the ground state will have a volume change as well as an energy discontinuity. We conclude that the transition from $L1_0$ to α IrV is probably weakly first order. We also examine the behavior of similar compounds, and show that the α IrV structures of both IrTi and RhTi are lower in energy than the experimentally observed high-temperature $L1_0$ structure.

Published by Elsevier B.V.

1. Introduction

A major goal of computational condensed matter physics is the determination of structural properties for compounds. Once the structure has been determined, other properties, e.g., strength, ductility, electronic properties (including superconductivity), magnetism, etc., can be determined. Several methods exist to attack this problem. One possibility is to exhaustively search an experimental database of known structures [1–3], determining the low energy structures for each composition of the target materials. Other methods use first-principles calculations on a small set of target structures to determine parameters which can be used to predict properties of more complex systems. These include the cluster expansion method [4–8], tight-binding parametrization methods [9,10], and atomistic potential methods [11]. Methods of the first type can be combined with methods of the second type for more thorough searches [12–14]. Using a more phenomenological approach, Pettifor [15] reordered the periodic table and showed that this grouped together binary compounds with similar structures, allowing some predictive capability.

These programs, can, however, only be implemented with a thorough knowledge of the behavior of compounds. Exhaustive searches of a database require an extensive database to search, including all structures which are known, or thought likely, to form for a target system. Parameterized methods may not be able to reach all regions of phase space, and also need a database of structures for testing [16,17]. Phenomenological methods may indicate trends, but may only relate compounds with similar high-temperature structures. For all methods, then, it is useful to look at less-common structures found in nature.

The α IrV structure, shown in Fig. 1, has so far only been observed in the prototype compound [18,19] and its neighbor in the periodic table, RhV [20,21]. This orthorhombic structure, space group $Cmmm$ (#65), can be viewed as a doubled unit cell distortion of the CsCl structure [22] or the tetragonal $L1_0$ structure, space group $P4/mmm$ (#123) [23]. Indeed, both the IrV and RhV phase diagrams [24] show the $L1_0$ structure as the ground state for vanadium-poor ($x=40$ –48%) [Ir,Rh]_{1-x}V_x, and vanadium-rich α IrV is known to transform to $L1_0$ at temperatures above 506 °C [23].

The seemingly straightforward transition pathway from $L1_0$ to α IrV was analyzed by Chen and Franzen [23] in the context of Landau theory: first, double the tetragonal $L1_0$ unit cell along the y and z directions, corresponding to a phonon at the R (0 1/2 1/2) point in reciprocal space. Second, construct the primitive base-centered

* Corresponding author. Tel.: +1 202 767 6579; fax: +1 202 404 7546.
E-mail address: Michael.Mehl@nrl.navy.mil (M.J. Mehl).

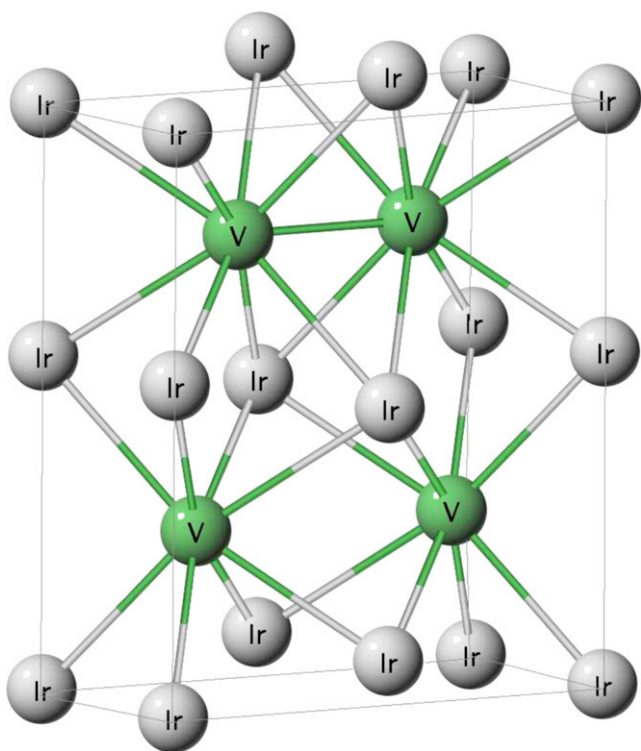


Fig. 1. The α IrV structure. The box indicates the boundaries of the full orthorhombic unit cell. In the $L1_0$ or (CsCl) structure the iridium atoms would be in a tetragonal (cubic) arrangement around each of the vanadium atoms.

orthogonal unit cell, and allow the two Ir atoms in the cell to move opposite each other along the z -axis, while the V atoms move along the y -axis. The resulting structure is symmetrically-equivalent to that of α IrV and, assuming a second-order phase transition, relaxes into the α IrV structure.

This simple picture is not quite accurate. A true second order transition, as described by Chen and Franzen, requires a continuous energy path from $L1_0$ to α IrV. Thus the energy of the $L1_0$ structure would be lowered by making an infinitesimal displacement of the type described above, corresponding to a phonon instability at the R point. We have performed first-principles density functional theory calculations for the phonon frequencies at the R point, both by the frozen phonon method [25] and by linear response [26–28]. We find that all of the modes here have real frequencies, i.e., they do not lead to an instability.

Thus the transition from the $L1_0$ phase to the α IrV phase does not proceed through the simple unit-cell doubling picture described above. Instead, as we shall show, the $L1_0$ phase has vibrational instabilities in another region of the Brillouin zone. This paper will discuss the structures arising from these instabilities, and explore the possibility that a second-order transition might go through one of those phases.

In Section 2 we show the results of density functional theory calculations for the energy and electronic structure of the α IrV and $L1_0$ phases of IrV, RhV, and some neighboring compounds. We show that in IrV and RhV the $L1_0$ structure has a relatively high electronic density of states at the Fermi level, and so the transition to α IrV has Jahn–Teller character [29]. We also find that IrTi and RhTi have lower energies in the α IrV structure than in the $L1_0$ structure.

In Section 3 we look at the phonon spectra of the α IrV and $L1_0$ phase. Not surprisingly, we find that the α IrV phase has no phonon instabilities. We do, however, find that the $L1_0$ structure is vibrationally unstable on and near the line $(x 1/4 1/2)$ in reciprocal space.

In Section 4 we use the frozen-phonon method on the unstable phonon modes to search for new structures which have lower energy than $L1_0$. Such a search is computationally bound, so we looked at all unit cells with eight atoms or less, and two structures with 32 atom unit cells. In this range we find no instability which relaxes to the α IrV phase, however it is not impossible that searching through larger unit cells would find such an instability, in which case the transition would indeed be second order. We do find several new structures, some of which have apparently never been seen in nature, and one which was previously known [21].

In Section 5 we discuss our results and thoughts on the order of the $L1_0$ – α IrV transition.

2. Energetics and electronic structure of the $L1_0$ and α IrV phases

All computations were made using the Kohn–Sham [30] formulation of density functional theory [31] with the Perdew–Burke–Ernzerhof [32] generalized gradient approximation. Depending on our needs, we used the Vienna *ab initio* Simulation Package (VASP) [33–35] with projector augmented-wave (PAW) potentials [36], or the *Quantum Espresso* (QE) package [37] with the supplied ultra-soft pseudopotentials for Ir, Rh, and V.

We used rather large plane wave cutoffs of 350 eV in VASP and 540 eV in QE to ensure convergence. We used Γ -centered k -point meshes with 729 and 369 points in the irreducible Brillouin zones of the $L1_0$ and α IrV structures, respectively. We summed over electronic states using a Fermi–Dirac distribution [38] with a temperature of 65 meV (0.005 Ry). Comparison with calculations for denser k -point meshes show that these values give energies converged to better than 0.5 meV/formula unit.

We show our results for IrV and RhV in Table 1 and Fig. 2. In both cases we see that the VASP PAW potentials and the QE ultra-soft pseudopotentials are in excellent agreement with one another, and in good agreement with experiment, within the usual errors of density functional theory in the generalized gradient approximation. In both compounds the α IrV state is below the $L1_0$ state by approximately 55 meV/formula unit, in agreement with experiment.

From experiment [23] we know that $L1_0$ is the preferred high temperature structure for α IrV. Using the COMSUBS routine from the ISOTROPY [39,40] package, we find that an orthorhombic distortion of the $L1_0$ structure reduces the symmetry from space group $P4/mmm$ to $Cmmm$, the space group of the α IrV structure. It is plausible to argue [23] that this lowering of symmetry is the pathway for the $L1_0 \rightarrow \alpha$ IrV phase transition. The symmetry-breaking character of the transition is evident from Fig. 3, where we plot the electronic density of states of both phases near the Fermi level. As we are only interested in the overall behavior of the density of states, we compute these curves by smearing out each eigenvalue found by VASP using a Fermi distribution at a temperature of 5 mRy. We see that at the Fermi level the density of states is twice as large in the $L1_0$ phase as it is in the α IrV phase. This is consistent with a Jahn–Teller-like symmetry breaking and phase transition [29]. As an aside, we also note that there is a minimum in the $L1_0$ density of states just above the Fermi level. This is consistent with the phase diagram of IrV [24], which shows that Iridium-rich IrV has the $L1_0$ structure. Assuming the additional Ir replaces V in the $L1_0$ structure, and using a rigid-band model, we can see how adding Ir to the system would raise the Fermi level and lower the density of states, leading to a more stable $L1_0$ phase. We find a similar, though less pronounced, state of affairs in RhV, as is also seen in Fig. 3.

We have investigated the possibility that the α IrV structure might be found in compounds neighboring IrV and RhV in the periodic table. The result of this investigation are shown in Table 2,

Table 1
Equilibrium lattice constants (in Å), atomic positions, and equilibrium bulk modulus (K_0 , in GPa) for the $L1_0$ and α IrV structures of IrV and RhV determined from experiment [18,20], VASP PAW calculations, and QE ultrasoft pseudopotential calculations. Note that we give the primitive tetragonal lattice parameters for the $L1_0$ structure, rather than the more-common face-centered tetragonal setting, so that when $c/a=1$ the $L1_0$ structure reduces to the cubic CsCl structure. The final row of the table shows the energy difference between the two phases (meV/formula unit).

	IrV			RhV		
	Exp.	VASP	QE	Exp.	VASP	QE
$L1_0$ structure						
a	2.749	2.755	2.762	2.754	2.739	2.745
c	3.651	3.677	3.668	3.599	3.660	3.648
K_0		272	277		230	
α IrV structure						
a	5.791	5.838	5.816	5.78	5.849	5.813
b	6.756	6.759	6.767	6.65	6.707	6.725
c	2.796	2.814	2.823	2.78	2.792	2.802
K_0		271	276		227	
Ir/Rh (4j)	0.22	0.216	0.216		0.214	0.215
V (4g)	0.28	0.296	0.297		0.296	0.297
ΔE		53.6	67.0		50.4	59.7

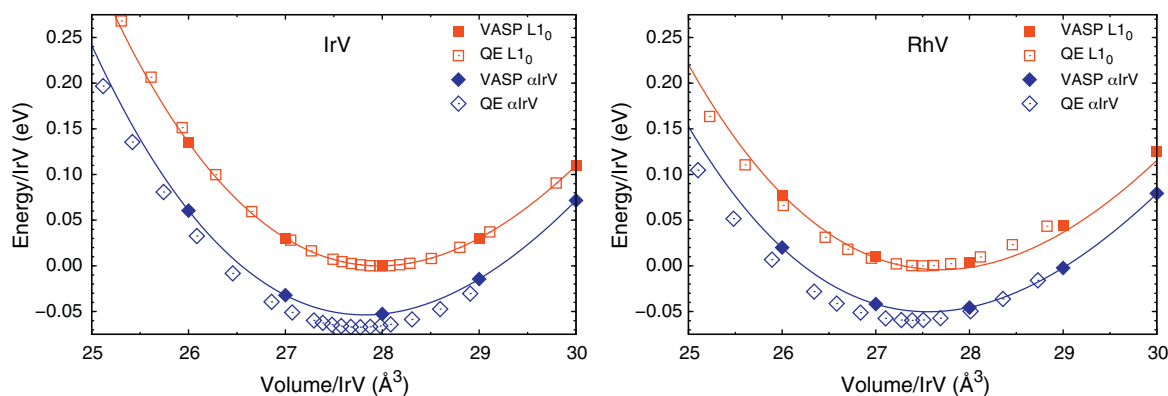


Fig. 2. Energy/volume curves for IrV and RhV in the $L1_0$ and α IrV structures, determined from VASP and QE calculations as discussed in the text. For ease of comparison we have set the minimum energy of the $L1_0$ phase to zero.

which shows the energy difference between the $L1_0$ and α IrV structure for several compounds. Most of these, (Ir,Rh)–(Nb,Ta,V) and CoV, have 14 electrons in the valence band. One, CoPt, has a ground state $L1_0$ structure. The other two, (Ir,V)Ti, were suggested by the original referee due to the fact that Pettifor's AB structure map [15] groups them together with the first class of compounds, and at temperatures above about 500 °C both compounds exhibit the $L1_0$ structure. In all cases, except for CoPt, we found that the α IrV structure was locally stable—that is, when we started from the structural parameters found for IrV in the α IrV structure, performed chemi-

cal alchemy to transform the atoms to the chosen compound, and relaxed the structure using VASP, we found a minimum energy structure distinct from the higher symmetry $L1_0$ structure. This suggests that the formation of the α IrV structure may be associated with features of the electronic density of states or Fermi surface arising from having 14 valence electrons per formula unit in the unit cell. We did not check the elastic and vibrational stability of the resulting structure. However the $L1_0$ structure was lower in energy for all compounds except IrV and RhV. Also, as shown in Fig. 4, for these compounds the density of states of the $L1_0$ structure is very

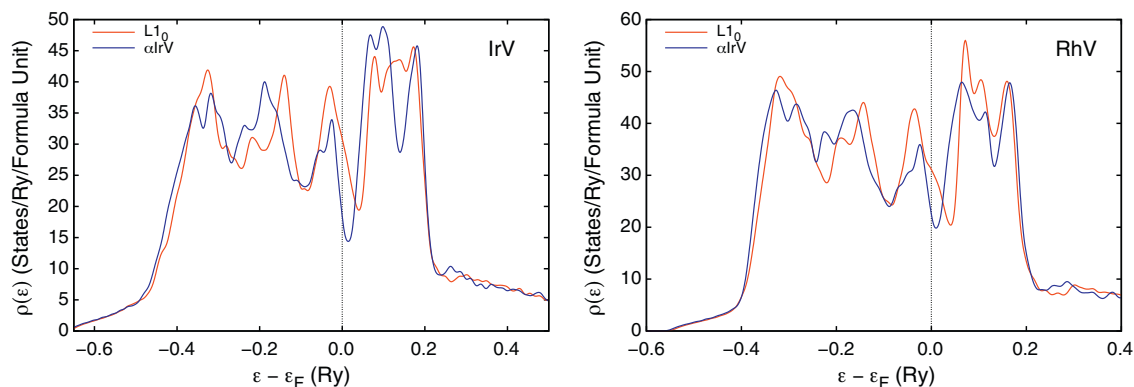


Fig. 3. Electronic density of states for the $L1_0$ (red) and α IrV (blue) phases of IrV (left) and RhV (right), found by smearing the eigenvalues computed by VASP using a Fermi–Dirac distribution at $T=65$ meV (5 mRy) [38]. (For interpretation of the references to color in this figure legend, the reader is referred to the web version of the article.)

Table 2

Energy difference, in meV per formula unit between the $L1_0$ and αIrV structures for the given compounds, as determined by VASP/PAW/PBE calculations. A positive number indicates that the $L1_0$ structure is lower in energy. An energy difference of zero indicates that the αIrV structure relaxes into the $L1_0$ structure. Ground state structures are from the *ASM Online Handbook* [24]. Note that for IrTi and RhTi we find the αIrV structure to be lower in energy than the listed ground state. The ordering of the Ir and Rh compounds follows Pettifor's AB structure map [15].

Compound	IrTi	IrTa	IrNb	Ir V
Ground state	$L1_0$		$L1_0$	αIrV
ΔE	-31.8	79.9	59.0	-53.6
Compound	RhTi	RhTa	RhNb	Rh V
Ground state	$L1_0$		$L1_0$	αIrV
ΔE	-27.3	70.6	50.1	-50.4
Compound	CoV	CoPt		
Ground State	$D8_b$	$L1_0$		
ΔE	25.3	0		

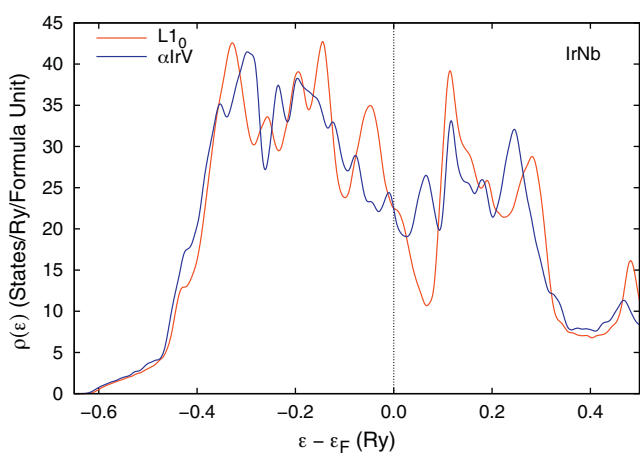


Fig. 4. Electronic density of states of the ground-state $L1_0$ and hypothetical αIrV phases of IrNb, found by smearing the eigenvalues computed by VASP.

near to that of the αIrV structure, precluding a Jahn–Teller lowering of the energy with decreased symmetry.

IrTi and RhTi are of course the exceptions to the 14 valence electron rule, as there are only 13 valence electrons per formula unit in the unit cell. However, Pettifor [15] maps both compounds to the same region of the AB structure map as IrV and RhV. We find that the αIrV structure is lower in energy than $L1_0$ in both cases, and so the $L1_0$ structure, which is observed experimentally for both compounds above about 500° C [24], cannot be the ground state. This is not unexpected, as *Pearson's Handbook* [41] gives limited information about low temperature monoclinic structures for both compounds. We will explore the details of both IrTi and RhTi in a later paper.

3. Stability of the $L1_0$ and αIrV phases

A system is stable, or metastable, only if it has real phonon frequencies for all k -points and modes.¹ Since the elastic constants are related to the long-wavelength behavior of the acoustic phonons [43] this implicitly includes the Born stability criteria [44]. This is fortunate, since the orthorhombic αIrV structure would require us to compute nine elastic constants.

To check the stability of the αIrV phase and the possible meta-stability of the $L1_0$ phase we computed phonon frequencies

¹ Acoustic phonons at Γ are guaranteed to vanish because of translational symmetry.

throughout the respective Brillouin zones using linear response [26–28], as implemented in the *Quantum Espresso* package PHon code [37]. Phonon frequencies were computed on a reciprocal space grid (“ q -points”) using an $8 \times 8 \times 4$ mesh for the $L1_0$ structure (45 points in the irreducible Brillouin zone) and a $6 \times 6 \times 4$ mesh for the αIrV structure (39 points). Linear response calculations at these points yield a reciprocal-space dynamical matrix. These matrices are transformed into a real-space dynamical matrix which can be used to compute phonon frequencies over the entire Brillouin zone.

This approach can lead to aliasing at points off of the q -point mesh. To check that this does not occur we also performed frozen-phonon calculations [25], wherein we construct a supercell commensurate with the given q -point and measure the change in energy as a function of atomic displacement within the supercell. To do this we used the program FROZSL, part of the ISOTROPY package [39,40], with atomic displacements of 0.1 Bohr. Electronic structure calculations were then performed with the same energy cutoff as the original unit cell, and when possible the same k -point mesh, albeit folded back into the smaller Brillouin zone associated with the supercell.

In the following, in interest of saving space, we only show the results for IrV. Our calculations for RhV show a similar pattern.

Fig. 5 shows the phonon frequencies of the equilibrium structure of αIrV . High symmetry points and lines are labeled according to the convention of Miller and Love [42], and can be generated automatically [45]. All the phonons have real frequencies, confirming that αIrV is at least a metastable structure for IrV, as suspected. There is no evidence of any aliasing in these calculations.

Fig. 6 shows the phonon frequencies of the $L1_0$ phase of IrV, along symmetry lines labeled according to the convention of Miller and Love [42]. We show results of frozen phonon calculations, showing good agreement between the two techniques, even off the linear response q -mesh. As expected, there are regions of reciprocal space with imaginary phonon frequencies. Surprisingly, this region is not near the R point ($0 \ 1/2 \ 1/2$) as described by Chen and Franzen [23], but along and near a line from the midpoint of the U line to the midpoint of the S line, as shown in more detail in the second panel of the figure. We will discuss the implications of this instability in the next section.

4. Searching for low energy structures

The previous section showed that the αIrV structure is the ground state (or, at least, a low-energy metastable state) of IrV, while the $L1_0$ structure is unstable to phonons along and near the line ($x \ 1/4 \ 1/2$) in the Brillouin zone, but not at the R point, where the phonon modes are real, invalidating the second-order phase

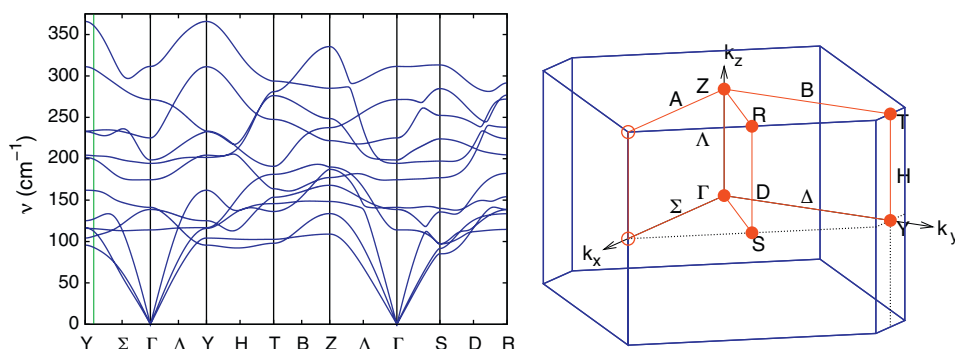


Fig. 5. The base-centered orthorhombic α IrV structure. Left: Phonon frequencies IrV at equilibrium, determined using the linear response method with ultrasoft pseudopotentials from the *Quantum Espresso* package. Right: First Brillouin zone. Symmetry lines are described by the notation of Miller and Love [42].

transition scenario of Chen and Franzen [23]. In this section we will look to see if it is possible to find another continuous transition path from $L1_0$ to α IrV.

In the frozen phonon method, we displace atoms from their equilibrium sites in a supercell consistent with the phonon wave vector and in directions which maintain the symmetry of the phonon mode. The frequency of the mode is then directly related to the square root of the curvature of the energy as a function of atom displacement. A mode with an imaginary frequency will then as a matter of course be related to a supercell calculation which has a negative curvature, leading to supercells with energy lower than the original state. These structures can then be relaxed, leading to new, or at least different, structures.

As an example of this, consider the unstable $L1_0$ phonon at the point $(1/4\ 1/4\ 1/2)$ on the high symmetry “S” line. The linear response calculations find an imaginary frequency of 81 cm^{-1} . We investigated the possible lower energy structures associated with this mode by using the FROZSL code from the ISOTROPY package [39,40] to generate the supercells and atomic displacements corresponding to each mode at the point. This package tells us that this point has phonons in three irreducible representations, each with two associated modes. For each representation we run three total energy calculations for displacements of the atoms in different directions, with the maximum displacement of 0.1 Bohr. The energy differences between these structures and the ground state are used to determine the dynamical matrix at this point, and the mode frequencies.

For the equilibrium $L1_0$ parameters found in Table 1, the S_3 irreducible representation (in the notation of Miller and Love [42]) has one mode with an imaginary frequency of 74 cm^{-1} . (The discrep-

ancy between linear response and frozen phonon calculations is due to the use of different k-point meshes and the anharmonicity of the mode. For our purposes we are only interested in showing that the mode is unstable in both cases, and so will not try to refine the calculations to improve the agreement between the two.)

Diagonalizing the dynamical matrix allows us to find a supercell with displaced atoms which has an energy lower than the $L1_0$ phase. This supercell has space group $Cmmm$ (#65), and with the appropriate choice of origin has Ir atoms at the (4e) and (4h) Wyckoff positions, and V atoms at the (2a), (2b), and (4j) positions. This is crystallographically equivalent to the intermetallic Ga_3Pt_5 structure [46], and we will refer to it as such. Upon relaxation we find a minimum energy structure which has approximately the same density as, and an energy $20.5\text{ meV/formula unit}$ below, the relaxed $L1_0$ structure of Table 1. Note that this is still well above the energy of the α IrV structure.

In a similar fashion, if we look at the phonons at $(0\ 1/4\ 1/2)$, on the “U” line, we find an imaginary U_3 mode with a frequency of 70 cm^{-1} . This mode leads to another supercell with space group $Cmmm$, but now the Ir atoms are on the (4e) and (4g) Wyckoff sites, while the V atoms occupy a pair of (4j) Wyckoff sites. The relaxed structure again has a density comparable to $L1_0$, but its energy is only $11.0\text{ meV/formula unit}$ below the $L1_0$ structure minimum. In the discussion below will refer to this structure as $Cmmm$.

Neither the Ga_3Pt_5 nor the $Cmmm$ structure will relax to the ground state α IrV structure. However, both structures have imaginary frequency long-wavelength optical mode phonons. If we venture away from the Γ point we will have to deal with frozen-

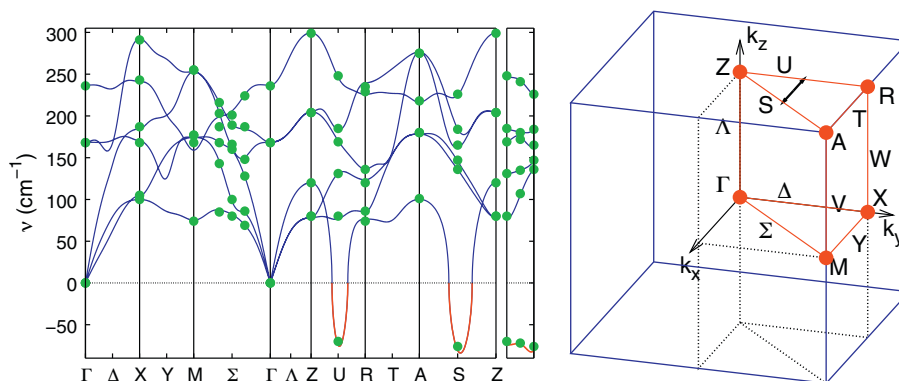


Fig. 6. The tetragonal $L1_0$ structure. Left: Phonon frequencies for IrV at its minimum energy structure, determined using the linear response method, using ultrasoft pseudopotentials from the *Quantum Espresso* package. Frequencies below zero (and in red) are unstable modes which actually have imaginary frequencies. The dots represent calculations using the frozen phonon method with displacements computed by FROZSL. The second panel shows the frequencies along the line $(x\ 1/4\ 1/2)$. Right: First Brillouin zone, with symmetry lines labeled according to the notation of Miller and Love [42]. The arrow from U to S indicates the region of unstable phonons. (For interpretation of the references to color in this figure legend, the reader is referred to the web version of the article.)

Table 3

Structural, energy, and vibrational stability results for the structures of IrV discussed in this paper. All calculations use the QE pseudopotentials discussed in the text. “Source” indicates the origin of the unit cell, either from experiment or an unstable phonon in the indicated structure. “Atoms” is the number of atoms in the primitive cell. Lattice constants are given in the standard crystallographic convention, e.g. the lattice constants of the full orthorhombic cell are given for the Cmmm and Cmcmm space groups. All primitive cells have $\alpha = \gamma = 90^\circ$. The rows “Ir” and “V” give the Wyckoff positions of the atoms. “Volume” is the minimum energy volume of the structure per formula unit, in (\AA^3). “Energy” is the energy of the structure below the $L1_0$ structure, in meV/formula unit.

Structure	$L1_0$	Cmmm	Cmcmm
Source	Exp.	$U_3(0\ 1/4\ 1/2)$ $L1_0$ phonon	$\Lambda_3(0\ 0\ 1)$ Cmmm phonon
Space group	$P4/mmm$	Cmmm	Cmcmm
Atoms	2	8	32
a (\AA)	2.762	7.260	7.198
b (\AA)	2.762	11.110	11.166
c (\AA)	3.668	2.774	11.136
β	90	90	90
Ir	(1a)(000)	(4e)(1/4 1/4 0) (4g)(.267 0 0)	(4d)(1/4 1/4 0) (4e)(.269 0 0) (4g)(.273 .254 1/4) (4g)(.268 .002 1/4)
V	(1d)(1/2 1/2 0)	(4j)(0 .364 1/2)(4j)(0 .115 1/2)	(4f)(0 .358 .134) (4f)(0 .632 .117) (4f)(0 .123 .132) (4f)(0 .895 .117)
Volume	27.97	27.97	27.97
Energy	0	10.98	20.61
Stability	Unstable	Unstable	Unknown

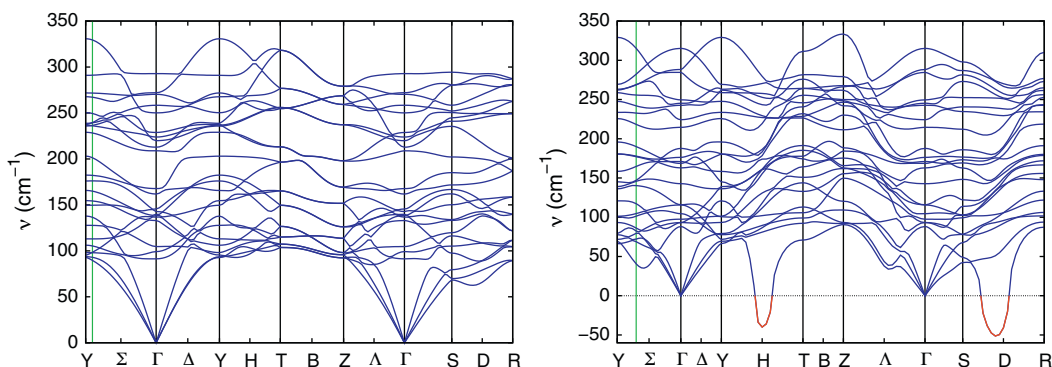


Fig. 7. Linear-response phonon spectra of two eight-atom unit cells derived from unstable phonon modes of $L1_0$ IrV. Left: The metastable Rh_5V_3 structure. Right: The Amm_2 structure with Ir atoms at two (4d) Wyckoff positions and V atoms at four (2b) Wyckoff positions. The imaginary frequencies of the unstable modes are shown as negative frequencies and highlighted in red. (For interpretation of the references to color in this figure legend, the reader is referred to the web version of the article.)

Table 4

Continuation of Table 3.

Structure	Ga_3Pt_5	Amm_2	Imm_2
Source	$S_3(1/4\ 1/4\ 1/2)$ $L1_0$ phonon	Γ_3^- Cmmm phonon	$H_1(1/4\ 0\ 0)$ Amm_2 phonon
Space group	Cmmm	Amm_2	Imm_2
Atoms	8	8	32
a (\AA)	7.222	2.788	7.176
b (\AA)	7.800	7.146	11.144
c (\AA)	3.974	11.230	11.190
β	90	90	90
Ir	(4e)(1/4 1/4 0) (4h)(.273 0 1/2)	(4d)(0 .230 .752) (4d)(0 .270 .998)	(4c)(.256 0 .252) (8e)(.268 2.50 .252) (4c)(0.223 0 .752) (4c)(.256 0 .998) (8e)(.268 .250 .998) (4c)(.223 0 .498)
V	(2a)(0 0 0) (2b)(1/2 1/2 0) (4j)(0 .218 1/2)	(2b)(1/2 0 .352) (2b)(1/2 0 .625) (2b)(1/2 0 .125) (2b)(1/2 0 .899)	(4d)(0 .131 .352) (4d)(0 .381 .355) (4d)(0 .132 .625) (4d)(0 .384 .625) (4d)(0 .130 .125) (4d)(0 .380 .125) (4d)(0 .131 .898) (4d)(0 .381 .895)
Volume	27.98	27.97	27.96
Energy	20.25	24.15	25.12
Stability	Unstable	Unstable	Unknown

Table 5
Continuation of Tables 3 and 4.

Structure	Cm	Rh ₅ V ₃	αIrV
Source	Δ ₁ (0 1/4 0) Amm2 phonon	Γ ₄ ⁻ Ga ₃ Pt ₅ phonon	Exp.
Space group	Cm	Amm2	Cmmm
Atoms	32	8	4
a (Å)	13.303	4.070	5.816
b (Å)	11.147	7.029	6.767
c (Å)	6.652	7.822	2.823
β	65.3	90	90
	(2a)(.999 0.504)		
	(2a)(.265 0.974)		
	(2a)(.485 0.534)		
	(2a)(.755 0.994)		
	(2a)(.870 0.256)		
Ir	(2a)(.140 0.715)	(4d)(0.219.724)	(4j)(0.216 1/2)
	(2a)(.360 0.276)	(4e)(1/2.281.001)	
	(2a)(.626 0.745)		
	(4b)(.992.249.521)		
	(4b)(.260.252.983)		
	(4b)(.365.748.267)		
	(4b)(.133 251.729)		
V	(4b)(.178 130.344)		
	(4b)(.175.380.362)		
	(4b)(.312.134.625)	(2a)(0 0.032)	
	(4b)(.312.385.625)	(2a)(0 0.457)	(4g)(.297 0 0)
	(4b)(.064.125.117)	(2b)(1/2 0.218)	
	(4b)(.060.375.133)	(2b)(1/2 0.793)	
	(4b)(.447.130.906)		
	(4b)(.450.380.888)		
Volume	27.97	27.97	27.78
Energy	25.67	41.14	67.25
Stability	Unknown	Metastable	Ground state

phonon calculations on unit cells having hundreds of atoms, so we will only examine the unstable modes at Γ in both structures.

First consider the imaginary frequency Γ_4^- mode of the Ga₃Pt₅ structure. It is associated with a supercell of space group *Amm2* (#38), with Ir atoms at the (4d) and (4e) Wyckoff sites and V atoms on pairs of (2a) and (2b) sites. This structure is crystallographically equivalent to the Rh₅V₃ structure [21,47] and will be referred to by that name. The relaxed structure is 41.1 meV/formula unit below the L1₀ structure, with similar density. This structure is metastable, as seen in the linear-response phonon spectrum plotted on the left-hand side of Fig. 7.

The second structure, derived from the unstable Γ_3^- mode of *Cmmm*, again with space group *Amm2* (#38), puts the Ir atoms on two (4d) sites and the V atoms on four distinct (2b) sites. The relaxed structure has an energy 24.1 meV/formula unit below the L1₀ structure, again with a similar density. This structure has not been found in the intermetallic literature. It is vibrationally unstable, as can be seen from the phonon spectrum on the right-hand side of Fig. 7.

The four structures Ga₃Pt₅, Rh₅V₃, *Cmmm* and *Amm2* are the only structures with eight or fewer atoms in the primitive cell which can be generated by relaxing the unstable phonon modes of the L1₀ structure. If we wish to examine larger unit cells, we can continue along this line of research *ad infinitum*, or until we find a supercell where the atoms relax to the ground state αIrV structure, a supercell with energy below the ground state structure, or we run out of computational resources. In most cases, including this one, we will reach the latter limit first. We did compute the relaxed energies of two supercells associated with unstable phonon modes in the *Amm2* structure, and one with an unstable mode of the *Cmmm* structure. These structures had thirty-two atoms in the supercell, and energies below the parent structure but above the metastable Rh₅V₃ structure.

Tables 3–5 summarize all of the calculations discussed here, including the structural derivation, space group, lattice constants, atomic positions, energy, and stability.

5. Discussion

We have shown by direct calculation that the transition from the L1₀ to the αIrV structure of both IrV and RhV is a result of a Jahn–Teller driven distortion of the high-symmetry unit cell. This distortion does not result from a zone-doubling unstable phonon at the R point of the L1₀ Brillouin zone, and so the simple Landau theory picture does not hold. This does not completely eliminate the possibility that the transition is second order, for we found an entire region of reciprocal space, in and around the line (x 1/4 1/2), where the L1₀ structure has vibrational instabilities. We examined several of those instabilities, and found that they lead to numerous new structures, most of which have yet to be seen in ordered intermetallic systems and most of which are vibrationally unstable. The only phase which we found that is metastable is the experimentally observed Rh₅V₃ phase, albeit in a 50–50 composition.

However, none of the unstable structures shows any sign of relaxing into the ground state structure. In fact, looking at Tables 2–4, we see that all of the structures except αIrV have approximately the same volume, 27.97 Å³/formula unit in IrV. The ground state αIrV structure, on the other hand, has a somewhat smaller volume, 27.78 Å³/formula unit. While this may seem insignificant, the volume change from one phase to another is a signal of a first-order transition, although only weakly first order here.

This paper also shows a mechanism for generating new candidate intermetallic phases: look for vibrationally unstable modes in a high energy structure, construct a supercell which will mimic that mode within the frozen-phonon calculation, and relax the cell. Using this method we found five new structures, as well as one, Rh₅V₃, which had been seen before but which we had not been aware of until this research started. Many more new structures can undoubtedly be derived from just this system, but further research in this area is currently restricted by the time needed to search the Brillouin zone of a given crystal. For the eight atom supercells computing the phonon spectrum at 45 q-points with a reason-

able number (≤ 64) of processors took days to weeks to complete, depending on the symmetry of the crystal. Calculating the phonons for larger unit cells will of course take longer, although we will have fewer q-points to consider, alleviating some of the $O[N^3]$ increase due to the larger unit cell. One of our research goals will be to construct a “set-and-forget” mechanism which will search the Brillouin zone of an initial structure (here $L1_0$) find all unstable modes with supercells containing a given number of atoms, relax those modes, and repeat, until all such structures have been found. Even restricting ourselves to all possible binary intermetallics [1] this will require a Grand Challenge computational program.

Finally, we found that IrTi and RhTi have a lower energy in the α IrV structure than in the $L1_0$ structure. This shows that Pettifor mapping, while useful in showing related compounds, can only be a guideline to determining new structures, and must be augmented by other techniques in order to find the true ground state behavior of compounds. We will discuss these interesting compounds in a later paper.

Acknowledgments

We thank the anonymous referee for suggesting that we look at the behavior of RhTi, and for the Pettifor reference [15], which led us to look at IrTi as well. We also thank Ohad Levy, Michal Jahnátek and Wahyu Setyawan for fruitful discussions.

M.J. Mehl is supported by the United States Office of Naval Research (ONR). S. Curtarolo acknowledges support by ONR (N00014-07-1-0878, N00014-07-1-1085, N00014-09-1-0921, and N00014-10-1-0436), and the United States National Science Foundation (NSF) (DMR-0639822). G.L.W. Hart is grateful for support from the NSF through grants DMR-0650406 and DMR-0908753. Many of the computations reported here, including all of the VASP calculations, were performed at the Air Force Research Laboratory Department of Defense Supercomputing Resource Center, Wright-Patterson Air Force Base, Dayton OH, under a grant from the DoD High Performance Computing Modernization Program.

Finally, the authors particularly wish to thank Prof. Harold Stokes for use of his ISOTROPY package.

References

- [1] S. Curtarolo, D. Morgan, K. Persson, J. Rodgers, G. Ceder, Predicting crystal structures with data mining of quantum calculations, *Phys. Rev. Lett.* 91 (13) (2003) 135503.
- [2] D. Morgan, G. Ceder, S. Curtarolo, High-throughput and data mining with ab initio methods, *Meas. Sci. Technol.* 16 (1) (2005) 296–301.
- [3] S. Curtarolo, G.L.W. Hart, W. Setyawan, M.J. Mehl, M. Jahnátek, R.V. Chepulskii, O. Levy, D. Morgan, Aflow, Software for High-throughput Calculation of Material Properties, 2010, URL <http://materials.duke.edu/afLOW.html>.
- [4] J.M. Sanchez, F. Ducastelle, D. Gratias, Generalized cluster description of multicomponent systems, *Physica A* 128 (1984) 334–350.
- [5] D. de Fontaine, Cluster approach to order-disorder transformations in alloys, *Solid State Phys.* 47 (1994) 33–176.
- [6] A. Zunger, First-principles statistical mechanics of semiconductor alloys and intermetallic compounds, in: P.E.A. Turchi, A. Gonis (Eds.), *Statics and Dynamics of Alloy Phase Transitions*, NATO ASI Series, Ser. B, Plenum Press, New York, 1994, pp. 361–419.
- [7] A. van de Walle, G. Ceder, Automating first-principles phase diagram calculations, *J. Phase Equilib.* 23 (2002) 348.
- [8] D. Lerch, O. Wieckhorst, G.L.W. Hart, R.W. Forcade, S. Müller, Constructing cluster expansions for arbitrary lattices from minimal user input, *Model. Simul. Mater. Sci. Eng.* 17 (2009) 055003.
- [9] M.J. Mehl, D.A. Papaconstantopoulos, Applications of a tight-binding total-energy method for transition and noble metals: elastic constants, vacancies, and surfaces of monatomic metals, *Phys. Rev. B* 54 (7) (1996) 4519–4530.
- [10] H. Haas, C.Z. Wang, M. Fähnle, C. Elsässer, K.M. Ho, Environment-dependent tight-binding model for molybdenum, *Phys. Rev. B* 57 (3) (1998) 1461–1470.
- [11] M.S. Daw, M.I. Baskes, Embedded-atom method: derivation and application to impurities, surfaces, and other defects in metals, *Phys. Rev. B* 29 (12) (1984) 6443–6453.
- [12] O. Levy, G.L.W. Hart, S. Curtarolo, Uncovering compounds by synergy of cluster expansion and high-throughput methods, *J. Am. Chem. Soc.* 132 (13) (2010) 4830–4833.
- [13] O. Levy, R.V. Chepulskii, G.L.W. Hart, S. Curtarolo, The new face of rhodium alloys: revealing ordered structures from first principles, *J. Am. Chem. Soc.* 132 (2) (2010) 833–837.
- [14] O. Levy, G.L.W. Hart, S. Curtarolo, Structure maps for hcp metals from first-principles calculations, *Phys. Rev. B* 81 (17) (2010) 174106.
- [15] D.G. Pettifor, *Bonding Structure of Molecules and Solids*, Clarendon Press, Oxford, 1995.
- [16] G.L.W. Hart, R. Forcade, Generating derivative structures: algorithm and applications, *Phys. Rev. B* 77 (2008) 224115.
- [17] G.L.W. Hart, R. Forcade, Generating derivative structures from multilattices: application to hcp alloys, *Phys. Rev. B* 80 (2009) 014120.
- [18] B.C. Giessen, N.J. Grant, New intermediate phases in transition metal systems. II, *J. Less-Common Met.* 18 (1965) 1080–1081.
- [19] B.C. Giessen, P.N. Dangel, N.J. Grant, New phases in the vanadium–iridium system and a tentative constitution diagram, *J. Less-Common Met.* 13 (1) (1967) 62–70.
- [20] R.M. Waterstrat, R.C. Manuszewski, The vanadium–rhodium constitution diagram, *J. Less-Common Met.* 52 (2) (1977) 293–305.
- [21] R.M. Waterstrat, B. Dickens, The crystal structure of V3Rh5, *J. Less-Common Met.* 31 (1) (1973) 61–67.
- [22] W.B. Pearson, *The Crystal Chemistry and Physics of Metals and Alloys*, Wiley-Interscience, New York, London, Sydney, Toronto, 1972.
- [23] B. Chen, H.F. Franzen, A second-order phase transition in v0.54ir0.46, *J. Less-Common Met.* 159 (1990) 343–347.
- [24] H. Baker (Ed.), *Alloy Phase Diagram*, ASM Handbooks Online, ASM International, 1991, URL <http://www.asmmaterials.info/>.
- [25] B.M. Klein, R.E. Cohen, Anharmonicity and the inverse isotope effect in the palladium–hydrogen system, *Phys. Rev. B* 45 (21) (1992) 12405–12414.
- [26] S. Baroni, P. Giannozzi, A. Testa, Green’s-function approach to linear response in solids, *Phys. Rev. Lett.* 58 (18) (1987) 1861–1864.
- [27] S. Baroni, S. de Gironcoli, A.D. Corso, P. Giannozzi, Phonons and related crystal properties from density-functional perturbation theory, *Rev. Mod. Phys.* 73 (2) (2001) 515–562.
- [28] X. Gonze, Adiabatic density-functional perturbation theory, *Phys. Rev. A* 52 (2) (1995) 1096–1114.
- [29] S. Lee, R. Hoffmann, BCC and FCC transition metals and alloys: a central role for the Jahn–Teller effect in explaining their ideal and distorted structures, *J. Am. Chem. Soc.* 124 (17) (2002) 4811–4823.
- [30] W. Kohn, L.J. Sham, Self-consistent equations including exchange and correlation effects, *Phys. Rev.* 140 (4A) (1965) A1133–A1138.
- [31] P. Hohenberg, W. Kohn, Inhomogeneous electron gas, *Phys. Rev.* 136 (3B) (1964) B864–B871.
- [32] J.P. Perdew, K. Burke, M. Ernzerhof, Generalized gradient approximation made simple, *Phys. Rev. Lett.* 77 (18) (1996) 3865–3868.
- [33] G. Kresse, J. Hafner, *Ab initio* molecular dynamics for open-shell transition metals, *Phys. Rev. B* 48 (17) (1993) 13115–13118.
- [34] G. Kresse, J. Hafner, *Ab initio* molecular-dynamics simulation of the liquid-metal/amorphous-semiconductor transition in germanium, *Phys. Rev. B* 49 (20) (1994) 14251–14269.
- [35] G. Kresse, Ph.D. thesis, Technische Universität Wien, Vienna, 1993.
- [36] G. Kresse, D. Joubert, From ultrasoft pseudopotentials to the projector augmented-wave method, *Phys. Rev. B* 59 (3) (1999) 1758–1775, doi:10.1103/PhysRevB.59.1758.
- [37] P. Giannozzi, S. Baroni, N. Bonini, M. Calandra, R. Car, C. Cavazzoni, D. Ceresoli, G.L. Chiarotti, M. Cococcioni, I. Dabo, A. D. Corso, S. de Gironcoli, S. Fabris, G. Fratesi, R. Gebauer, U. Gerstmann, C. Gougousis, A. Kokalj, M. Lazzeri, L. Martin-Samos, N. Marzari, F. Mauri, R. Mazzarello, S. Paolini, A. Pasquarello, L. Paulatto, C. Sbraccia, S. Scandolo, G. Sclauzero, A. P. Seitsonen, A. Smogunov, P. Umari, R. M. Wentzcovitch, Quantum espresso: a modular and open-source software project for quantum simulations of materials, *J. Phys.: Condens. Matter* 21 (39) (2009) 395502.
- [38] M. J. Gillan, Calculation of the vacancy formation energy in aluminium, *J. Phys.: Condens. Matter* 1 (4) (1989) 689–711.
- [39] H.T. Stokes, D.M. Hatch, B.J. Campbell, ISOTROPY, <http://stokes.byu.edu/isotropy.html> (2007).
- [40] B.J. Campbell, H.T. Stokes, D.E. Tanner, D.M. Hatch, Isodisplace: a web-based tool for exploring structural distortions, *J. Appl. Crystallogr.* 39 (2006) 607–614.
- [41] P. Villars, L.D. Calvert (Eds.), *Pearson’s Handbook of Crystallographic Data for Intermetallic Phases*, 2nd ed., ASM International, Materials Park, OH, 1991.
- [42] S.C. Miller, W.F. Love, *Tables of Irreducible Representations of Space Groups and Co-representations of Magnetic Space Groups*, Pruetz, Boulder, 1967.
- [43] C. Kittel, *Introduction to Solid State Physics*, 7th ed., John Wiley & Sons, New York, 1996, Chapter 3, pp. 80–95.
- [44] M. Born, K. Huang, *Dynamical Theory of Crystal Lattices*, Oxford at the Clarendon Press, Oxford, 1966, pp. 11–13.
- [45] W. Setyawan, S. Curtarolo, High-throughput electronic band structure calculations: challenges and tools, *Comp. Mat. Sci.* 49 (2) (2010) 299–312.
- [46] K. Schubert, S. Bhan, W. Burkhardt, R. Gohle, H.G. Meissner, M. Pötzschke, E. Stolz, *Einige strukturelle Ergebnisse an metallischen Phasen* (5), *Naturwissenschaften* 47 (13) (1960) 303.
- [47] P. Villars, L.D. Calvert (Eds.), *Pearson’s Handbook of Crystallographic Data for Intermetallic Phases*, vol. IV, 2nd ed., ASM International, Materials Park, OH, 1991, pp. 5091.